

Electronic Supplementary Information

Size effects on Rhodium nanoparticles related to hydrogen-storage capability

Chulho Song,^a Anli Yang,^a Osami Sakata,^{*abc} L. S. R. Kumara,^a Satoshi Hiroi,^b Yi-Tao Cui,^d Kohei Kusada,^e Hirokazu Kobayashi,^e and Hiroshi Kitagawa^{ef}

^a Synchrotron X-ray Station at SPring-8, Research Network and Facility Services Division, National Institute for Materials Science, 1-1-1 Kouto, Sayo, Hyogo 679-5148, Japan

^b Synchrotron X-ray Group, Research Center for Advanced Measurement and Characterization, National Institute for Materials Science, 1-1-1 Kouto, Sayo, Hyogo 679-5148, Japan

^c Department of Innovative and Engineered Materials, Tokyo Institute of Technology, 4259-J3-16, Nagatsuta, Midori, Yokohama 226-8502, Japan

^d Synchrotron Radiation Laboratory, The Institute for Solid State Physics, The University of Tokyo, 1-490-2 Kouto, Shingu-cho Tatsuno, Hyogo 679-5165, Japan

^e Division of Chemistry, Graduate School of Science, Kyoto University, Kitashirakawa Oiwake-cho, Sakyo-ku, Kyoto 606-8502, Japan

^f INAMORI Frontier Research Center, Kyushu University, 744 Motooka, Nishi-ku, Fukuoka 819-0395, Japan

*Corresponding author: E-mail: SAKATA.Osami@nims.go.jp

SUPPORTING NOTE 1. TEM images¹ and particle size distributions of Rh NPs

Supplementary Figure 1 shows the TEM images for Rh NPs. TEM images were recorded on a JEM-200CX or Hitachi HT7700, operated at 200 or 100 kV accelerating voltage, respectively. The particle size distribution of Rh NPs was shown in Supplementary Figure 2. The mean diameters of the nanoparticles were determined from the TEM images to be (a) 2.4 ± 0.5 , (b) 4.0 ± 0.7 , (c) 7.1 ± 1.2 , and (d) 10.5 ± 0.8 , respectively. Numbers that follow the \pm sign represent estimated standard deviations.

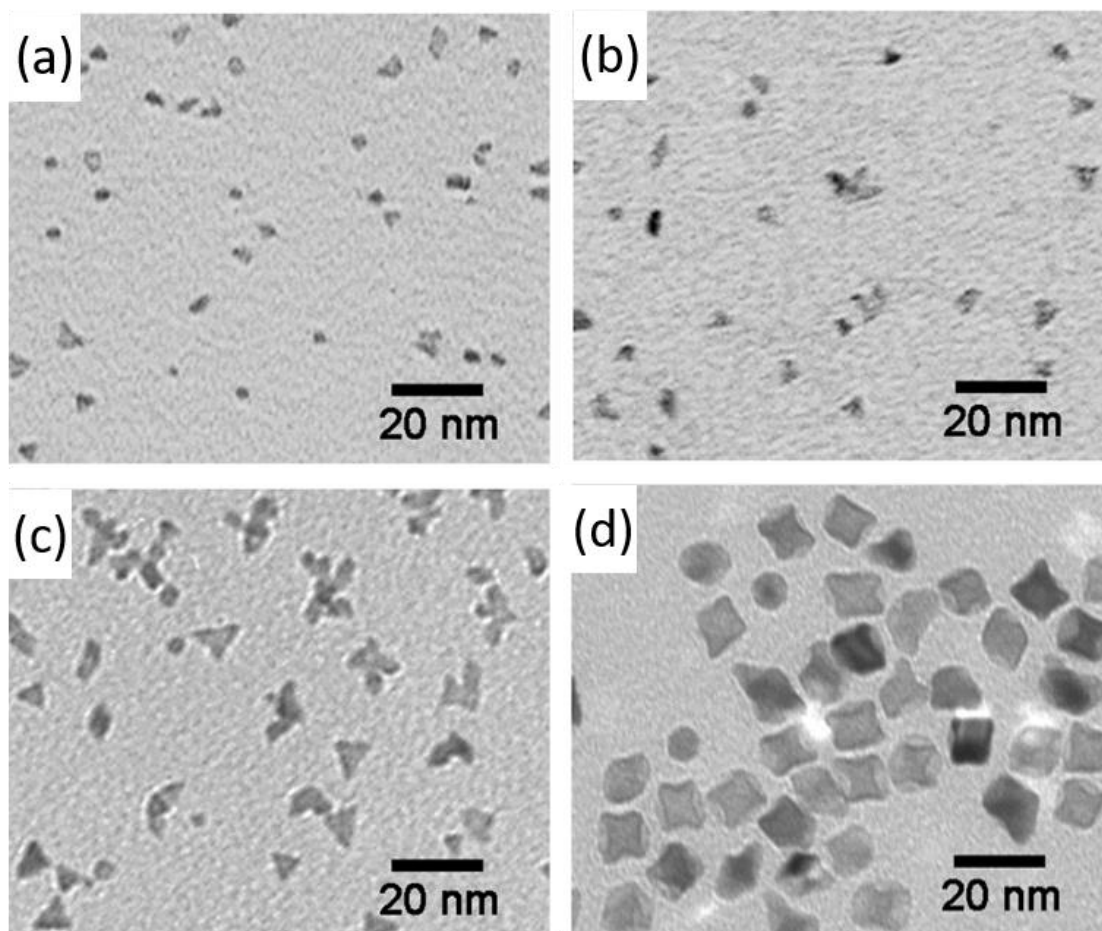


Figure S1. TEM images of Rh NPs¹
: (a) 2.4 nm, (b) 4.0 nm, (c) 7.1 nm, (d) 10.5 nm.

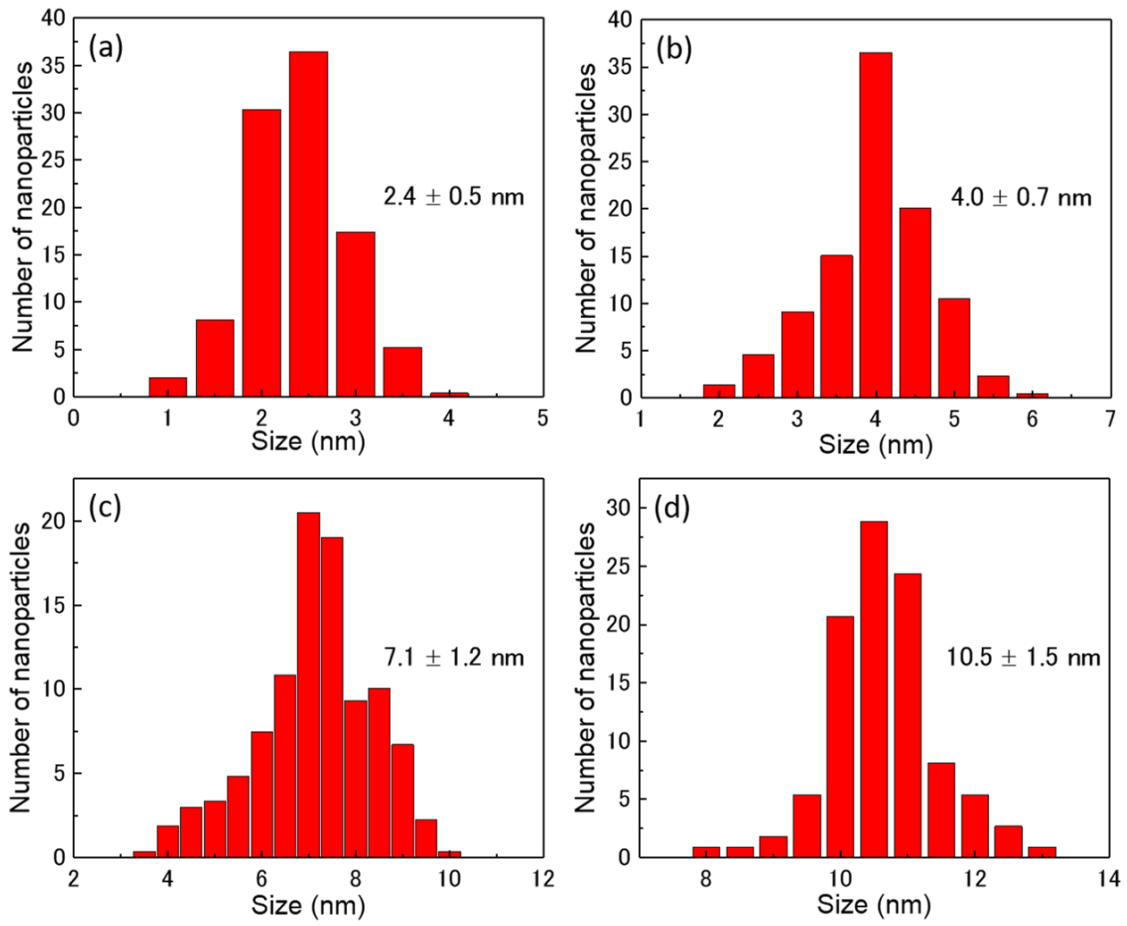


Figure S2. Particle size distributions of Rh NPs
: (a) 2.4 nm, (b) 4.0 nm, (c) 7.1 nm, (d) 10.5 nm.

SUPPORTING NOTE 2. Hydrogen pressure-composition (PC) isotherms for Rh NPs

Hydrogen pressure-composition (PC) isotherms for the Rh NPs were measured with a volumetric technique using a pressure composition temperature (PCT) apparatus (Suzuki Shokan Co., Ltd. Japan). The pressure sensor was a INFICON SKY Model CR090 and its range was from 1.33 to 133000 Pa. The purity of the hydrogen was 99.999 %, oxygen < 1 ppm. The weights of the measured samples were more than 100 mg as the amount of the metal. As a pre-treatment before the absorption process, a volume measurement of the NPs was performed with helium. Because the amount of hydrogen absorption tends to be overestimated from the 1st PC isotherm owing to reduction of the particle surface, we measured each PC isotherm more than three times. After confirming whether the 2nd and 3rd measurements exhibited reproducibility, we used the 2nd PC isotherm dataset. For absorption measurements, the pressure during the introduction of the hydrogen was raised in 23 steps (50, 100, 200, 300, 400, 500, 600, 700, 800, 900, 1000, 1500, 2000, 3000, 4000, 5000, 6000, 7000, 8000, 9000, 10000, 15000, 20000 Pa). The next step was not initiated until the differential pressure had settled within 15 Pa after 5 min of hydrogen introduction and the PC isotherm data had been collected. Above 2×10^{-2} MPa, the pressure was automatically set and the measurements were performed using the same conditions. During desorption measurements, the next step was initiated after the differential pressure had settled to the same conditions as the corresponding absorption measurements by automatic control. The PC isotherms of Rh NPs are described in Supplementary Ref. 1.

SUPPORTING NOTE 3. Rietveld analysis for fcc Rh NPs

Supplementary Figure 3 shows the results of the Rietveld refinement of the XRD patterns of the fcc Rh NPs at room temperature. The experimental high-energy XRD patterns of the fcc Rh NPs exhibited well-defined Bragg peaks that could be indexed to a cubic unit cell.

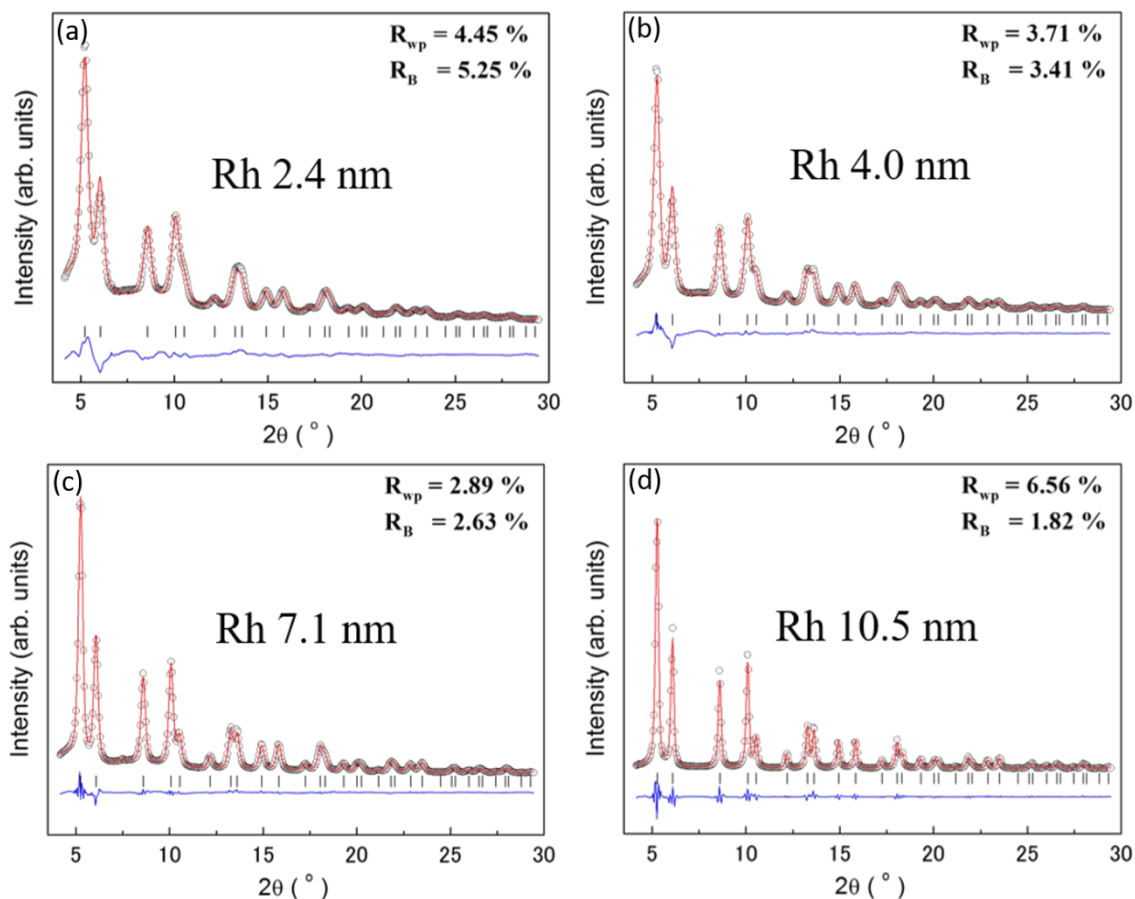


Figure S3. Refinement results for fcc Rh NPs at room temperature
: (a) 2.4 nm, (b) 4.0 nm, (c) 7.1 nm, (d) 10.5 nm.

SUPPORTING NOTE 4. Crystalline domain size

Supplementary Figure 4 shows the relationship between the average crystalline domain size and particle size. The domain size was calculated from the Scherrer equation, $D = K\lambda/\beta\cos\theta$, where D is the average crystalline domain size, K ($= 0.9$ if nanoparticles are assumed to be spherical) is the shape factor, λ ($= 0.202 \text{ \AA}$) is the X-ray wavelength, β is the line-broadening of the observed peak, expressed as the FWHM in radians, and θ is the Bragg angle. The average crystalline domain sizes of the Rh NPs were obtained using fifteen Bragg peaks (from 111 to 600). The accuracy of the Scherrer equation is limited by the uncertainty in β . The error in β , determined from the results of the Rietveld analysis, was approximately 10%. For Rh NPs, the average domain size decreased linearly with decreasing particle size. This result means that the particle size of Rh NP can be determined from the magnitude of the Rh domain size, not the number of small Rh domains (similar to the case of fcc Ru NPs²), and consistent with the expectation from Fig. 2(a).

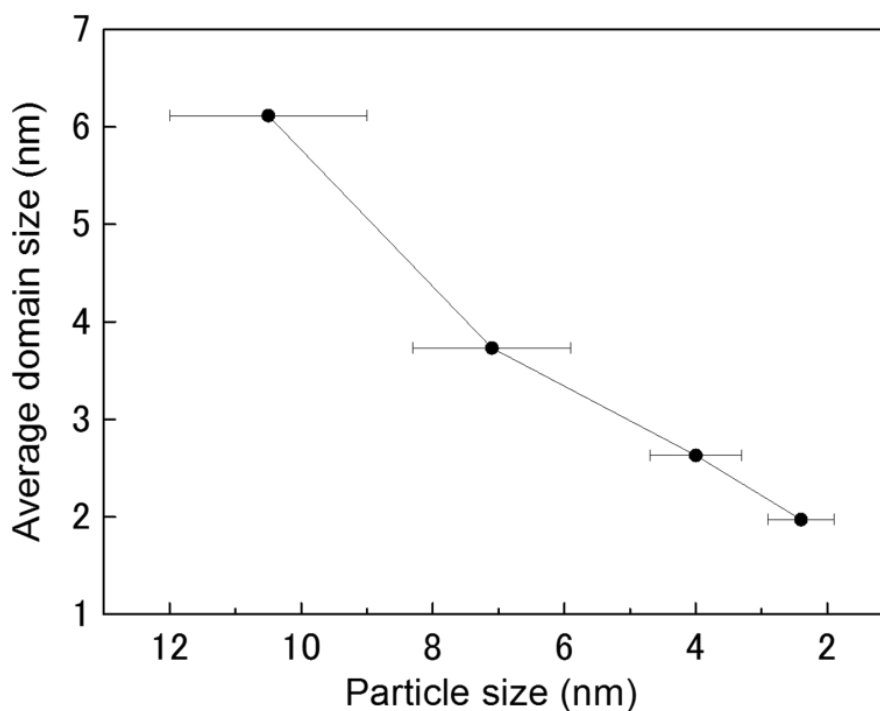


Figure S4. Average crystalline domain size as a function of particle size.

SUPPORTING NOTE 5. Calculation of the number of domains (N) for evaluating the surface area of the crystalline domain ($A_{surface}$) for Rh NPs

The number of domains for each Rh NPs were calculated based on the same weight of 1.0 mg. Molar mass of Rh is 102.91 *g/mol*. Therefore, the number of Rh atoms per 1.0 mg can be calculated by the following equation (eq. S1).

$$\text{Number of Rh atoms per 1.0 mg} = \frac{1.0 \times 10^{-3} \text{g}}{102.91 \text{g}} \times 6.02 \times 10^{23} \approx 5.85 \times 10^{18} \quad (\text{eq. S1})$$

The number of unitcell per domain can be calculated by the following equation (eq. S2).

$$\text{Number of unitcell per domain} = \frac{V_{domain}}{\text{unit volume}} = \frac{\frac{4}{3}\pi(\frac{D}{2})^3}{\text{unit volume}} \quad (\text{eq. S2})$$

where V_{domain} is the volume of crystalline domain, and D is the average crystalline domain size. Considering the number, which is four, of Rh atoms included in unitcell for Rh NPs, the number of Rh atoms per 1 domain can be simply calculated by the following equations (eq. S3)

$$\text{Number of Rh atoms per domain (for fcc structure)} = \text{Number of unitcell per domain} \times 4 \quad (\text{eq. S3})$$

Finally, the number of domain (N) per 1.0 mg for Rh NPs can be calculated from eq. S1 and S3.

$$N = (\text{Number of Rh atoms per 1.0 mg}) \div (\text{Number of Rh atoms per domain}) \quad (\text{eq. S4})$$

SUPPORTING NOTE 6. X-ray absorption fine structure (XAFS) spectra

Supplementary Figure 5 shows the experimental Rh *K*-edge XAFS spectra for Rh foil and Rh NPs. There were no significant changes in the energy position of the Rh *K*-edge and peaks, although peak broadening owing to the size effect was observed. The amplitude of the 1st peak increased with decrease in particle size. In contrast, that of the 2nd peak decreases with decreasing particle size. The white line (1st peak) area in *K*-edge is directly related to the transition of a 1s core electron to a bound state such as an empty or partially filled molecular orbital³. An increase in white line area corresponds to an increase in the density of empty states capable of accepting an electron. This indicates that XAFS spectra gradually changed from that of the Rh⁰ metal to that of the Rh^{δ+} cation with decrease in particle size.

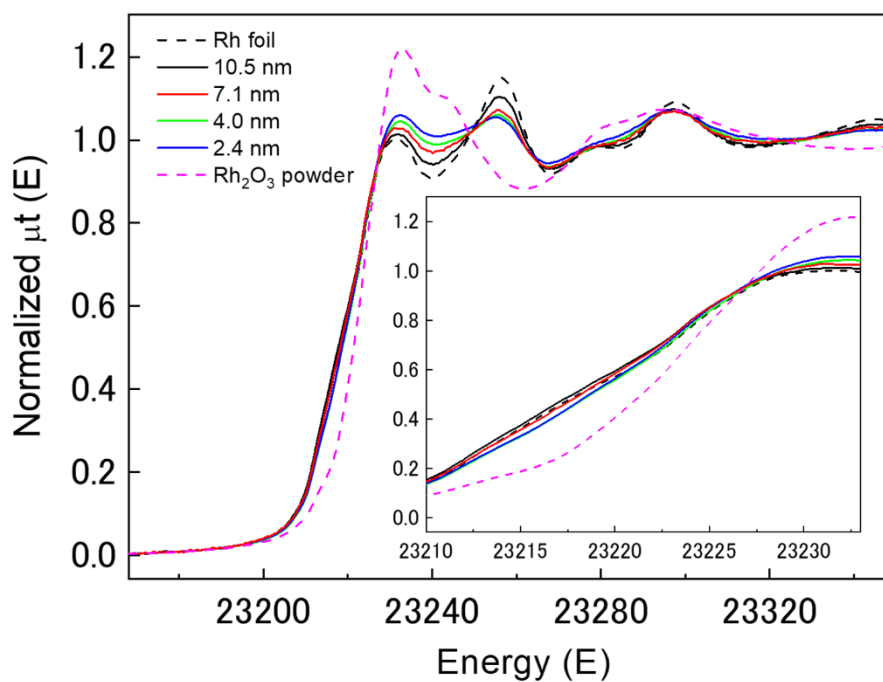


Figure S5. Experimental Rh *K*-edge XAFS spectra for Rh foil, Rh₂O₃ powder, and Rh NPs.

SUPPORTING NOTE 7. Reverse Monte Carlo (RMC) simulation and bond-orientational order (BOO) parameter

Supplementary Figure 6 shows the RMC experimental and simulated structure factor data sets for Rh NPs (2.4, 4.0, 7.1 nm). The 3-dimensional structure models of Rh NPs were generated by RMC modelling method using RMC_POT software⁴ furnished for the case of non-periodic boundary conditions. RMC models of Rh NPs were constructed by 526 (2.4 nm), 2434 (4.0 nm), 13610 (7.1 nm) total atoms in a spherical configuration. The diameter of spherical samples was determined from TEM images in figure S1. As shown in Supplementary figure 6, the simulated total scattering factor $S(Q)$ and experimental data shows a good agreement for Rh NPs. From the cavity analysis using a Dirichlet-Voronoi construction, we determined the volume fraction of cavities for Rh NPs.

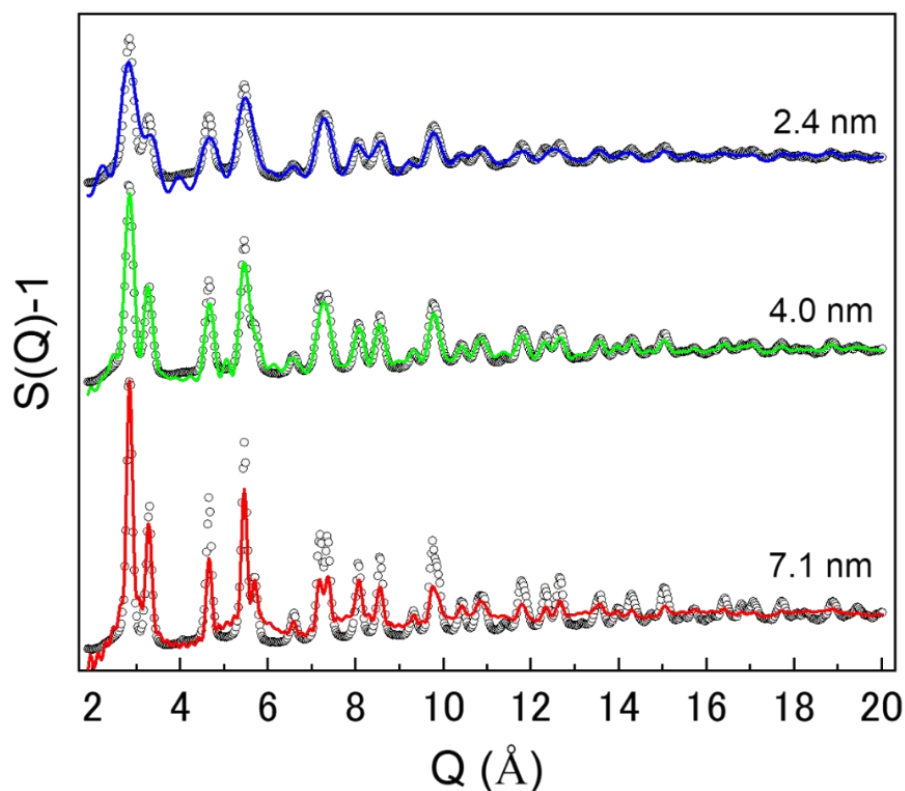


Figure S6. Experimental and RMC simulated X-ray total structure factor $S(Q)-1$.

Supplementary Figure 7 shows the distribution of the bond-orientational order (BOO) parameter^{5, 6} in the q_4 and q_6 , which was calculated from RMC structure modelling, for Rh NPs. The set of BOO parameters give us the information of the local structure, defined as,

$$q_l(i) = \sqrt{\frac{4\pi}{2l+1} \sum_{m=-l}^l \left| \frac{1}{N(i)} \sum_{j=1}^{N(i)} Y_{lm}(r_{ij}) \right|^2}$$

Here, $N(i)$ is the number of nearest neighbors of particle i , The functions Y_{lm} are the spherical harmonics and \mathbf{r}_{ij} is the vector from particle i to particle j . The values of q_4 and q_6 ($q_{4,ideal}$ and $q_{6,ideal}$) for an ideal fcc structure are 0.190 and 0.575, respectively⁶. These values were presented in the blue close star (see Supplementary Figure 7). We divided the whole volume of Rh NPs into a core part and a surface part. The surface part is 0.33 nm from the surface; the rest volume is the core part. We calculated the average value of q_4 and q_6 (\bar{q}_4 and \bar{q}_6) for the core part, surface part and the entire volume of Rh NPs as shown in Supplementary Table 1. The all values of \bar{q}_4 of Rh NPs were larger than the ideal value. In contrast, the all of value of \bar{q}_6 were smaller than the ideal value. To investigate the deviation between the ideal fcc structure and fcc Rh NPs, we apply to a parameter P_{BOO} ⁷ describing their difference from the ideal structure, defined as,

$$P_{BOO} = \sqrt{\left(\frac{\bar{q}_4}{q_{4,ideal}} - 1\right)^2 + \left(\frac{\bar{q}_6}{q_{6,ideal}} - 1\right)^2}$$

The detailed discussion of P_{BOO} is described in the main text (see Figure 4(c)).

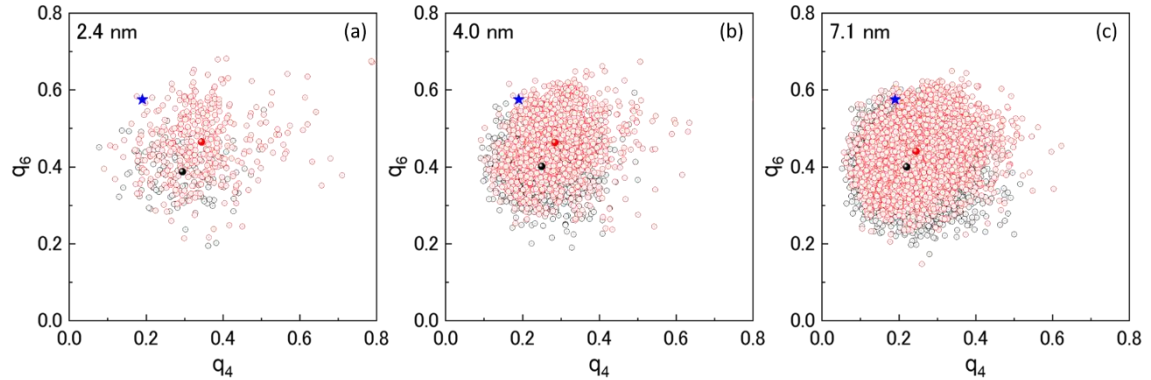


Figure S7. Distribution plane for the BOO parameters q_4 and q_6 of the fcc Rh NPs ((a) 2.4 nm, (b) 4.0nm, (c) 7.1 nm). The black and red open circles indicate a core and a surface part, respectively. The black and red close circles mark the average value of a core and a surface part for BOO parameter of fcc Rh NPs, respectively. The blue close star marks the BOO parameter for an ideal fcc structure.

Table S1: Average value of q_4 and q_6 (\bar{q}_4 and \bar{q}_6) for the core part, surface part and the entire volume of Rh NPs.

| Particle size/nm | Core | | Surface | | Total | |
|------------------|-------------|-------------|-------------|-------------|-------------|-------------|
| | \bar{q}_4 | \bar{q}_6 | \bar{q}_4 | \bar{q}_6 | \bar{q}_4 | \bar{q}_6 |
| 2.4 | 0.294 | 0.388 | 0.344 | 0.465 | 0.330 | 0.443 |
| 4.0 | 0.250 | 0.401 | 0.285 | 0.463 | 0.267 | 0.432 |
| 7.1 | 0.220 | 0.400 | 0.245 | 0.441 | 0.228 | 0.413 |

REFERENCES

- [1] Kusada, K.; Kobayashi, H.; Ikeda, R.; Morita, H.; Kitagawa, H. Changeover of the Thermodynamic Behavior for Hydrogen Storage in Rh with Increasing Nanoparticle Size. *Chem. Lett.* **2013**, *42*, 55-56.
- [2] Song, C. *et al.* Size dependence of structural parameters in fcc and hcp Ru nanoparticles using Rietveld refinement analysis of high-energy X-ray diffraction data. *Sci. Rep.* **2016**, *6*, 31400.
- [3] Thomas, J. M. *et al.* Principles and Practice of Heterogeneous Catalysis, VCH: Weinheim, 1997, 196
- [4] Gereben, O.; Petkov, V. Reverse Monte Carlo Study of Spherical Sample Under Non-Periodic Boundary Conditions: The Structure of Ru Nanoparticles Based on X-ray Diffraction Data. *J. Phys.: Condens. Matter* **2013**, *25*, 454211-454219.
- [5] Steinhardt, P. J.; Nelson, D. R.; Ronchetti, M. Bond-orientational order in liquids and glasses. *Phys. Rev. B* **1983**, *28*, 784-805
- [6] Mickel, W.; Kapfer, S. C.; Schroder-Turk, G. E.; Mrcke, K. Shortcomings of the bond orientational order parameters for the analysis of disordered particulate matter. *J. Chem. Phys.* **2013**, *138*, 044501
- [7] Seo, O. *et al.* Stacking fault density and bond orientational order of fcc ruthenium nanoparticles. *Appl. Phys. Lett.* **2017**, *111*, 253101 ,